Virtual SIMO Radar Modelling in Arrayed MIMO Radar

Harry Commin and Athanassios Manikas

Department of Electrical and Electronic Engineering, Imperial College London
South Kensington Campus, London, SW7 2AZ, UK
harry.commin@imperial.ac.uk
a.manikas@imperial.ac.uk

Abstract—In this paper, an equivalent 'virtual' SIMO (Single Input Multiple Output) radar representation of the MIMO radar system is established which enables the analysis of the full MIMO system geometry. Analytical expressions are derived to describe the key geometrical properties of the virtual array's manifold, which fully characterises the entire transmit-receive system geometry.

A new family of subarrayed collinear MIMO array structures is presented for obtaining uniform linear virtual arrays. It is shown that this reduces the required radar platform size by up to a half, compared to popular existing methods, without reducing virtual array aperture.

NOTATION

a, A	Scalar
$\underline{a}, \underline{A}$	Column Vector
$\mathbb{A}$	Matrix
$(\cdot)^T, (\cdot)^H$	Transpose and conjugate transpose
$\mathbb{I}_N$	$(N \times N)$ identity matrix
$\underline{1}_N$	$(N \times 1)$ vector of ones
$|\cdot|$	Absolute value
$\|\cdot\|$	Euclidean norm of vector
$\underline{a}^b$	Element-by-element power
$\exp(\underline{a})$	Element-by-element exponential
$\mathcal{E}\{\cdot\}$	Expectation operator
$\odot, \otimes$	Hadamard and Kronecker product

I. INTRODUCTION

An arrayed multiple input multiple output (MIMO) radar is a radar system which employs two antenna arrays: one to transmit and one to receive. For each of these arrays, the antenna elements are distributed in three-dimensional real space about a common reference point. More specifically, the focus of this paper is "collocated" MIMO radar (wherein transmit and receive arrays are sufficiently close together that target bearings are the same for both arrays) [1], as opposed to widely-spaced MIMO radar configurations [2].

Array signal processing in multiple-target MIMO radar is concerned with the task of exploiting the arrays' geometries (antenna locations) in order to detect, resolve and estimate the various parameters of multiple radar targets. In this context, detection performance is defined as the capability of the system to correctly estimate the number of targets, K. Then, resolution performance refers to the system's ability to subsequently yield unique parameter estimates for those K targets. Estimation performance is then determined by the accuracy of those parameter estimates, following successful resolution.

The key to designing and analysing an array system in general lies in understanding the array manifold, which is a geometric object that completely characterises the array. Specifically, the array manifold is defined as the locus of all the response vectors (manifold vectors) of the array over the feasible set of signal/target parameters. A branch of mathematics dedicated to the investigation of the properties of such geometric objects (curves, surfaces, etc.), is differential geometry. The profound and fundamental importance of the array manifold's shape has been extensively investigated in the literature using differential geometry [3]. However, until now, these methods have been applied only to the receiver array of the array system. Therefore, in MIMO radar (where there also exists an arrayed transmitter), it has not previously been possible to fully characterise the whole transmit-receive system geometry within such a framework.

In this paper, an equivalent 'virtual' SIMO (Single Input Multiple Output) representation of the MIMO radar system is established which allows direct analysis of the full MIMO system geometry. The virtual array concept has already been introduced in the MIMO radar literature (see, for example, [4,5]). However, existing theory focuses on specific methods for explicitly obtaining and exploiting the output of the virtual array. For example, by exploiting transmit signal diversity with respect to code division [6], frequency division [7] or time division [8]. In this paper, a more general approach is taken, whereby the properties of the virtual SIMO system are identified and analysed without making any assumptions about how this structure might be exploited in practice. Using this general virtual SIMO representation, a study of the fundamental geometric properties of the MIMO configuration is then presented.

The virtual array representation also provides useful insight into the problem of MIMO radar array design (i.e. determining where physical antennas should be placed). To this end, an investigation of the popular uniform linear virtual array is presented. In particular, a new family of subarrayed collinear

MIMO array configurations are introduced which allow the physical size of the MIMO radar platform to be significantly reduced, compared to traditional approaches.

The remainder of the paper is organised as follows. In Section II, the MIMO radar received signal model is derived. In Section III, the equivalent virtual SIMO radar representation of the MIMO radar system is derived and analysed. In Section IV, a novel approach to uniform linear virtual array design is proposed. The paper is concluded in Section V.
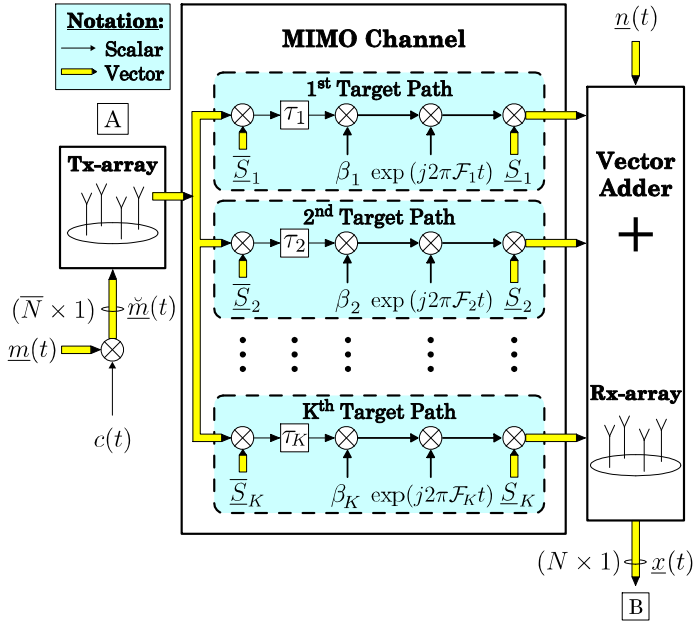
II. MIMO RADAR SYSTEM MODEL

Fig. 1: Baseband representation of the MIMO radar system.

Consider the arrayed MIMO radar system of Figure 1, which employs an array of $\overline{N}$ transmitting antennas and an array of N receiving sensors. The two arrays are assumed to be collocated, i.e. they are located sufficiently close together in space that target bearings are the same for both arrays. The $\overline{N}$ elements of the transmit array are fed by the $(\overline{N} \times 1)$ vector of baseband transmit waveforms, $\breve{m}(t) \triangleq m(t)c(t)$, which are transmitted into the environment (see Point A in Figure 1) and assumed to propagate as plane waves. It is convenient to assume that $m(t)$ is (element-wise) unity power and independent of $c(t)$. Meanwhile, the power of $\breve{m}(t)$ is normalised to enforce a unity transmit power constraint.

The MIMO channel comprises K signal propagation paths, corresponding to the transmitted signal energy reflected back to the receiver via K radar targets. The signal return from the kth target has complex path fading coefficient β_k, while τ_k models the lack of synchronisation between transmitter and receiver due to the different target ranges. Doppler frequency is denoted $\mathcal{F}_k$ and is a known function of radial target velocity, v_k:

$$\mathcal{F}_k \triangleq -\frac{2v_k f_c}{c} \qquad (1)$$

where f_c denotes carrier frequency and c is the speed of light.

The $(N \times 1)$ complex vector $\underline{S}_k \triangleq \underline{S}(\theta_k, \phi_k)$ is the receiver array manifold vector (array response vector), which models the response of the receiver array to a plane-wave arrival from the direction parameterised by azimuth θ_k and elevation ϕ_k:

$$\underline{S}(\theta_k, \phi_k) \triangleq \exp\left(-j[\underline{r}_x, \underline{r}_y, \underline{r}_z]\underline{k}(\theta_k, \phi_k)\right) \qquad (2)$$

The receiver array's sensor locations (array geometry) are represented by the $(N \times 3)$ real matrix:

$$[\underline{r}_x, \underline{r}_y, \underline{r}_z] = [\underline{r}_1, \underline{r}_2, \ldots, \underline{r}_N]^T \in \mathcal{R}^{N \times 3} \qquad (3)$$

Similarly, using $(\bar{\cdot})$ to denote all equivalent parameters associated with the transmit array, $[\overline{r}_x, \overline{r}_y, \overline{r}_z]$, the transmit array manifold vector is denoted $\overline{S}_k \triangleq \overline{S}(\theta_k, \phi_k)$.

In Equation 2, $\underline{k}(\theta_k, \phi_k)$ is the wavenumber vector:

$$\underline{k}(\theta_k, \phi_k) \triangleq \frac{2\pi f_c}{c} \overbrace{[\cos(\theta_k)\cos(\phi_k), \sin(\theta_k)\cos(\phi_k), \sin(\phi_k)]}^{\underline{u}(\theta_k, \phi_k)} \qquad (4)$$

where $\underline{u}(\theta_k, \phi_k)$ is the (3×1) real unit vector pointing from (θ_k, ϕ_k) towards the origin. (Equivalently, for the transmitter's manifold vector, $\overline{u}(\theta_k, \phi_k) = -\underline{u}(\theta_k, \phi_k)$ points from the origin to (θ_k, ϕ_k)). Without loss of generality, phase origins of the transmit and receive arrays are defined at the centroids of the arrays.

The $(N \times 1)$ baseband signal at the receiver array output (in the presence of noise) can therefore be modelled as follows:

$$\underline{x}(t) = \sum_{k=1}^{K} \beta_k \exp(j2\pi\mathcal{F}_k t)\underline{S}_k \overline{S}_k^H \breve{m}(t - \tau_k) + \underline{n}(t) \qquad (5)$$

where the spatially and temporally white, zero-mean complex Gaussian additive noise is denoted by $\underline{n}(t)$, with covariance matrix:

$$\mathbb{R}_{nn} \triangleq \mathcal{E}\{\underline{n}(t)\underline{n}^H(t)\}$$
$$= \sigma_n^2 \mathbb{I}_N \qquad (6)$$

where σ_n^2 is the unknown noise variance.

III. THE VIRTUAL SIMO RADAR EQUIVALENT TO THE MIMO RADAR SYSTEM

A key challenge in MIMO radar is to determine how the transmit array geometry (described by $[\overline{r}_x, \overline{r}_y, \overline{r}_z]$) can be exploited effectively to enhance parameter estimation capability at the receiver. By contrast, the receiver array geometry is relatively straightforward to exploit in this sense, since each element of $\underline{x}(t)$ is known to correspond to a specific receive antenna. Therefore, (assuming a calibrated array) signals arriving at the receive antennas have a known response as a function of (θ, ϕ), as described by $\underline{S}(\theta, \phi)$. Consequently, a wide variety of parametric approaches can be applied to estimate (θ, ϕ), based upon this modelling.

One way of utilising transmit array geometry would therefore be to – in some sense – "virtually" transfer the transmit antennas across to the receiver. In this way, the output of a
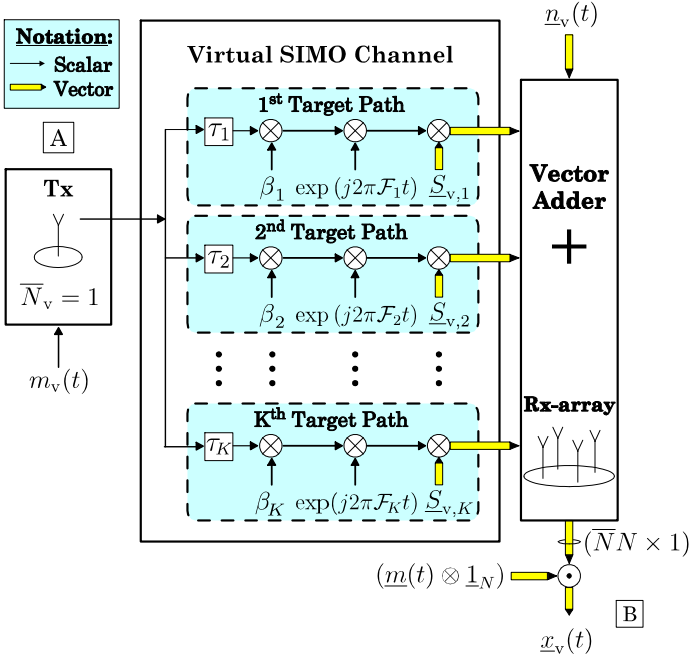
Fig. 2: Virtual SIMO radar equivalent of the MIMO radar system depicted in Figure 1.

virtual SIMO array could be exploited at the MIMO radar receiver whose response is a function of both $\underline{S}(\theta, \phi)$ and $\overline{S}(\theta, \phi)$.

The structure of the virtual SIMO received signal can be derived by noting that the MIMO $\underline{x}(t)$ can be rearranged as shown in Equation 7, below (the proof of which is given in Appendix A). From $\underline{x}_v(t)$ (in Equation 7), the structure of the equivalent virtual SIMO system can therefore be derived. This structure is depicted in Figure 2, wherein the virtual SIMO manifold vector has the form:

$$\underline{S}_{v,k} = \overline{S}_k^* \otimes \underline{S}_k \tag{8}$$

and the signal vector, $\underline{m}(t)$, has also been transferred from transmitter to receiver and applied (element-by-element) at the output of the virtual SIMO receiver. The virtual transmitted signal is:

$$m_v(t) = c(t) \tag{9}$$

The virtual noise is defined implicitly by the relationship:

$$\left(\underline{1}_{\frac{T}{N}} \otimes \mathbb{I}_N\right) \underline{n}_v(t) = \underline{n}(t) \tag{10}$$

It is straightforward to see that the virtual noise covariance matrix can be assumed to take the form:

$$\mathbb{R}_{n_v n_v} \triangleq \mathcal{E}\{\underline{n}_v(t)\underline{n}_v^H(t)\}$$
$$= \sigma_{n_v}^2 \mathbb{I}_N \tag{11}$$

from which it follows (using Equation 10) that:

$$\sigma_{n_v}^2 = \frac{1}{\overline{N}}\sigma_n^2 \tag{12}$$

From Equations 9 and 12, it is evident that both the signal and noise powers at a given virtual sensor is a factor of $\overline{N}$ smaller than in the MIMO radar system. This is to be expected, since the number of virtual sensors is greater by a factor of $\overline{N}$ and the total signal and noise energies must be the same in both systems. Importantly, the signal to noise ratios are equal in both systems:

$$\mathrm{SNR}_{v,k} = \mathrm{SNR}_k \tag{13}$$

Using Equation 8, the geometry of the virtual array can now be derived. Noting that $(\overline{S}^* \otimes \underline{S}) = (\overline{S}^* \otimes \underline{1}_N) \odot (\underline{1}_{\overline{N}} \otimes \underline{S})$, the virtual SIMO array sensor locations are given by:

$$[\underline{r}_{v,x}, \underline{r}_{v,y}, \underline{r}_{v,z}] \triangleq \left([\overline{r}_x, \overline{r}_y, \overline{r}_z] \otimes \underline{1}_N\right) + \left(\underline{1}_{\overline{N}} \otimes [\underline{r}_x, \underline{r}_y, \underline{r}_z]\right) \tag{14}$$

which can be viewed as a spatial convolution of the MIMO transmit and receive arrays.

Of course, in the actual observed MIMO signal vector, $\underline{x}(t)$, the signals at certain subarrays of the virtual array have been summed together, as reflected by the term $\left(\underline{1}_{\frac{T}{N}} \otimes \mathbb{I}_N\right)$.

A. Fundamental Performance Bounds of the Virtual SIMO Radar System

The fundamental detection, resolution and estimation performance bounds of a SIMO system were proven in [3] to be a function of array geometry and the finite sampling effect. In this respect, the array is fully characterised by the array manifold, which is defined as the locus of the array manifold vector over the feasible set of signal/target parameters. Meanwhile, the finite sampling effect is represented by an 'uncertainty hypersphere' whose radius is given by:

$$\sigma_e = \frac{1}{\sqrt{2\left(\mathrm{SNR} \times L\right)}} \tag{15}$$

Thus, by considering the circular approximation to the array manifold, it has been shown that the fundamental detection and resolution capabilities are characterised, respectively, by the following threshold separations:

$$\underline{x}(t) = \left(\underline{1}_{\frac{T}{N}} \otimes \mathbb{I}_N\right) \left(\underbrace{(\underline{m}(t) \otimes \underline{1}_N) \odot \sum_{k=1}^{K} \beta_k \exp(j2\pi\mathcal{F}t)\left(\overline{S}_k^* \otimes \underline{S}_k\right) c(t - \tau_k) + \underline{n}_v(t)}_{\triangleq \underline{x}_v(t) \in \mathbb{C}^{N\overline{N} \times 1}}\right) \tag{7}$$

$$\Delta p_{\text{det}} = \frac{1}{\dot{s}(\breve{p})} \left(\sigma_{e_1} + \sigma_{e_2} \right) \tag{16}$$

$$\Delta p_{\text{res}} = \frac{1}{\dot{s}(\breve{p})} \sqrt[4]{\frac{4}{\left(\hat{\kappa}_1^2(\breve{p}) - \frac{1}{N} \right)}} \left(\sqrt{\sigma_{e_1}} + \sqrt{\sigma_{e_2}} \right) \tag{17}$$

where $\Delta p \triangleq |p_2 - p_1|$ and $\breve{p} \triangleq \frac{p_1 + p_2}{2}$ denote, respectively, the separation and midpoint between two closely-spaced targets with locations parameterised by p_1 and p_2 (for some generic directional parameter, p, e.g. azimuth or elevation). Meanwhile, $\dot{s}(p)$ is the manifold's rate of change of arc length and $\kappa_1(p)$ denotes its principal curvature (where $\hat{\kappa}_1(p)$ also takes into account the inclination angle of the manifold). For notational brevity, dependence on directional parameter p will often be omitted from subsequent discussion.

It was shown in [3] that fundamental estimation performance can also be investigated through study of the Cramer-Rao bound in the context of array manifold geometry. However, this bound depends on assumptions as to whether each system parameter is random or deterministic, known or unknown. Estimation error bounds are therefore omitted from the present general discussion and the interested reader is referred to [9].

Following the methods outlined in [10, Equation 30] for evaluating the properties of extended array manifolds, it can be shown from Equation 14 that:

$$\dot{s}_{\text{v}} = \sqrt{\overline{N}\dot{s}^2 + N\dot{\overline{s}}^2} \tag{18}$$

$$\hat{\kappa}_{1,\text{v}} = \frac{1}{\dot{s}_{\text{v}}^2} \sqrt{\left(\left\| \underline{\ddot{A}}_{\text{v}}^2 \right\|^2 + \left\| \underline{\dddot{A}}_{\text{v}} \right\|^2 - \ddot{s}_{\text{v}}^2 \right) - \frac{\left(1\frac{T}{\overline{N}N} \underline{\dddot{A}}_{\text{v}}^3 \right)^2}{\dot{s}_{\text{v}}^2}} \tag{19}$$

where a dot over a symbol denotes differentiation with respect to p and we have defined $\underline{A}_{\text{v}}(p) \triangleq -[\underline{r}_{\text{v},x}, \underline{r}_{\text{v},y}, \underline{r}_{\text{v},z}]\underline{k}(p)$. Since $\hat{\kappa}_{1,\text{v}}$ will tend to be smaller than $\hat{\kappa}_1$ (because the virtual manifold lies on a hypersphere of significantly larger radius), it is important to confirm that resolution performance is dominated by the improvement in $\dot{s}_{\text{v}}$. Indeed, it can be shown that:

$$\dot{s}_{\text{v}}^4 \left(\hat{\kappa}_{1,\text{v}}^2 - \frac{1}{N_{\text{v}}} \right) \geq$$
$$\overline{N}\dot{s}^4 \left(\hat{\kappa}_1^2 - \frac{1}{N} \right) + N\dot{\overline{s}}^4 \left(\hat{\overline{\kappa}}_1^2 - \frac{1}{\overline{N}} \right) + 4\dot{\overline{s}}^2\dot{s}^2 \tag{20}$$

Due to space restrictions, a full proof of this inequality will be published elsewhere [11]. An illustrative example comparing $\dot{s}_{\text{v}}(\theta)$ and $\dot{s}(\theta)$ is given in Figure 3.

IV. Spatially Efficient Uniform Linear Virtual Array Design

From Equation 14, it is evident that a specific (desired) $\overline{N}N$-element virtual array geometry is not necessarily achievable via any possible arrangement of the available $\overline{N} + N$ physical MIMO antennas. Conversely, a given (achievable) virtual array geometry may be constructible via a multitude
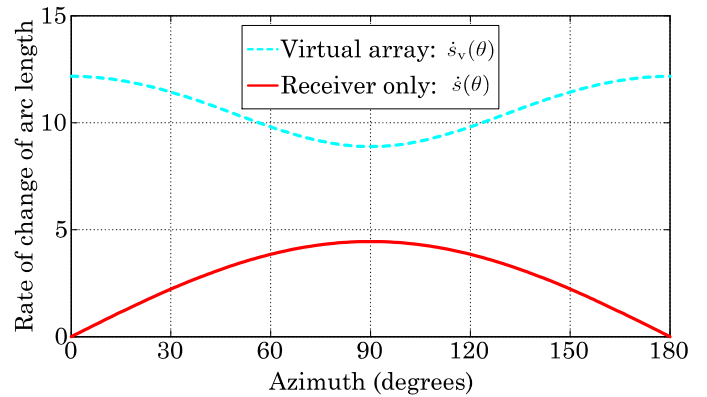

Fig. 3: Rate of change of arc length for the virtual array and receiver array, for a MIMO radar system with $[\overline{r}_x, \overline{r}_y, \overline{r}_z] = \begin{bmatrix} 0 & -1.5 & 0 \\ 0 & -0.5 & 0 \\ 0 & 0.5 & 0 \\ 0 & 1.5 & 0 \end{bmatrix}$ and $[\underline{r}_x, \underline{r}_y, \underline{r}_z] = \begin{bmatrix} -1 & 0 & 0 \\ 0 & 0 & 0 \\ 1 & 0 & 0 \end{bmatrix}$, for targets lying in the x-y plane. Total length of the virtual array's θ-curve is approximately 3.74 times larger than the receiver array's.

of different arrangements of the MIMO antennas. For these reasons, array design is not straightforward in MIMO radar. One achievable virtual array geometry that has received particular research interest is the "filled" ($\frac{\lambda}{2}$-spaced) uniform linear virtual array [6,12]. In this section, it will be shown that the traditional method for achieving a uniform linear virtual array makes inefficient use of the available space on the radar platform. Therefore, a new family of subarrayed collinear MIMO geometries is defined and shown to offer superior spatial efficiency.

The following notation is first defined to describe the desired $\overline{N}N$-element virtual array:

$$\underline{r}_{\text{v},x} = \underline{\text{ULA}}_{\overline{N}N} \tag{21}$$

where $\underline{\text{ULA}}_A$ denotes the x-coordinates of the A-element, $\frac{\lambda}{2}$-spaced uniform linear array (in units of $\frac{\lambda}{2}$):

$$\underline{\text{ULA}}_A \triangleq \left[-\frac{1}{2}(A-1), -\frac{1}{2}(A-1)+1, \ldots, \frac{1}{2}(A-1) \right]^T \tag{22}$$

Although this configuration is incapable of elevation estimation and can operate (unambiguously) across only $180°$ of azimuth, it does provide particularly powerful performance close to array broadside ($\theta \approx 90°$). Another advantage is the simplicity of analysis. Specifically, by adapting [13, Appendix B], system performance is characterised by the following quantities:

$$\dot{s}_{\mathrm{v}}(\theta) = \frac{\pi \sin(\theta)}{\sqrt{12}} \sqrt{\overline{N} N \left(\overline{N}^2 N^2 - 1 \right)} \qquad (23)$$

$$\hat{\kappa}_{1,\mathrm{v}}(\theta) = \sqrt{\frac{3(3\overline{N}^2 N^2 - 7)}{5\overline{N} N (\overline{N}^2 N^2 - 1)}} \qquad (24)$$

The traditional method found throughout the MIMO radar literature for obtaining this structure of $\underline{r}_{\mathrm{v},x}$ is:

$$\overline{r}_x = N\underline{\mathrm{ULA}}_{\overline{N}} \ \text{ and } \ \underline{r}_x = \underline{\mathrm{ULA}}_N \qquad (25)$$

or, by symmetry:

$$\overline{r}_x = \underline{\mathrm{ULA}}_{\overline{N}} \ \text{ and } \ \underline{r}_x = \overline{N}\underline{\mathrm{ULA}}_N \qquad (26)$$

However, it would not seem that alternative methods for obtaining the filled linear virtual array have been explored in detail. To this end, we define a new family of subarrayed configurations by noting that Equation 21 can be rewritten as:

$$
\underline{r}_{\mathrm{v},x} = \mathbb{1}_{\overline{N}} \otimes \overbrace{\overline{N}_{\mathrm{sub}}\underline{\mathrm{ULA}}_N}^{\underline{r}_x}
$$
$$
+ \underbrace{\left(\overline{N}_{\mathrm{sub}} N \left(\underline{\mathrm{ULA}}_{\overline{B}_{\mathrm{sub}}} \otimes \mathbb{1}_{\overline{N}_{\mathrm{sub}}} \right) + \left(\mathbb{1}_{\overline{B}_{\mathrm{sub}}} \otimes \underline{\mathrm{ULA}}_{\overline{N}_{\mathrm{sub}}} \right) \right)}_{\overline{r}_x} \otimes \mathbb{1}_N
$$
$$\tag{27}$$

where the transmit array has been separated into $\overline{B}_{\mathrm{sub}}$ subarray "blocks", each of which comprises $\overline{N}_{\mathrm{sub}} \triangleq \frac{\overline{N}}{\overline{B}_{\mathrm{sub}}}$ elements (and receiver array spacings have been increased accordingly). Alternatively, it could be the receiver array that is divided into subarrays, but the transmit array is considered here.

Note that the same virtual array is produced for any (integer) values of $\overline{N}_{\mathrm{sub}}$ and $\overline{B}_{\mathrm{sub}}$. Therefore, without affecting the fundamental direction-finding capabilities, we may freely choose values of $\overline{N}_{\mathrm{sub}}$ and $\overline{B}_{\mathrm{sub}}$ to gain advantages according to some other criterion. For example, it will now be shown that the physical size of the MIMO radar platform can be minimised, while maintaining maximum (filled) virtual array size.

To begin, we note (from Equation 14) that the sum of the apertures of the transmit and receive arrays is constrained to be equal to the virtual array aperture:
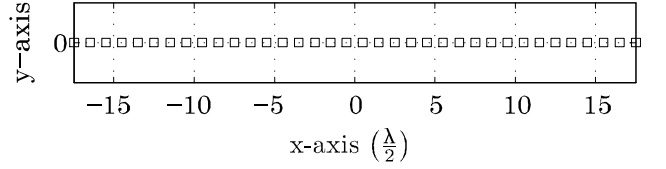
$$
\Delta r_{\mathrm{v},x} \triangleq \overbrace{\max\left(\underline{r}_{\mathrm{v},x}\right) - \min\left(\underline{r}_{\mathrm{v},x}\right)}^{\text{Virtual aperture}}
$$
$$
= \max\left(\overline{r}_x\right) + \max\left(\underline{r}_x\right) - \min\left(\overline{r}_x\right) - \min\left(\underline{r}_x\right)
$$
$$
= \underbrace{\left(\max\left(\overline{r}_x\right) - \min\left(\overline{r}_x\right)\right)}_{\text{Transmit aperture } \triangleq \Delta\overline{r}_x} + \underbrace{\left(\max\left(\underline{r}_x\right) - \min\left(\underline{r}_x\right)\right)}_{\text{Receive aperture } \triangleq \Delta r_x} \tag{28}
$$

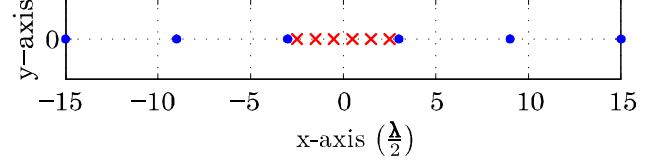where, from Equation 27, the respective MIMO apertures are:

$$\Delta\overline{r}_x = \overline{N} N - (N-1)\overline{N}_{\mathrm{sub}} - 1 \qquad (29)$$

$$\Delta r_x = (N-1)\overline{N}_{\mathrm{sub}} \qquad (30)$$
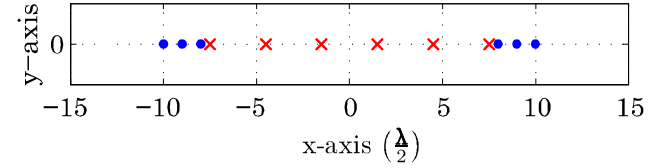
Therefore, in order to minimise the overall physical span of the $\overline{N} + N$ MIMO antennas, we simply place the transmit and receive arrays' centroids at the same point in space and then make their respective apertures as similar as possible.

(a) The desired 36-element filled uniform linear virtual array, which is produced by both Fig. 4(b) and Fig. 4(c).

(b) Traditional approach occupies 30 half-wavelengths.

(c) Proposed approach occupies 20 half-wavelengths.

Fig. 4: For $(\overline{N} \times N) = (6 \times 6)$, the proposed method reduces radar platform size by a third, compared to existing methods. A black square denotes a virtual SIMO sensor, blue '·' denotes a MIMO transmit antenna and red 'x' denotes a MIMO receive antenna.

Specifically, we obtain the $\overline{N}_{\mathrm{sub}}$ which minimises the absolute difference (squared) between the apertures:

$$\overline{N}_{\mathrm{sub}}^{\mathrm{opt}} \triangleq \left[\!\left[\arg\min_{\overline{N}_{\mathrm{sub}}} \left(\Delta\overline{r}_x - \Delta r_x\right)^2 \right]\!\right]_{\overline{N}} \qquad (31)$$

where $[\![\cdot]\!]_{\overline{N}}$ denotes rounding to the nearest integer factor of $\overline{N}$ (since a useful solution must provide integer values for $\overline{N}_{\mathrm{sub}}$ and $\overline{B}_{\mathrm{sub}}$). Simply rounding in this way is valid due to the symmetric, convex (parabolic) nature of the objective function in Equation 31. Equating the derivative of the objective function to zero then leads to:

$$\overline{N}_{\mathrm{sub}}^{\mathrm{opt}} = \left[\!\left[\frac{\overline{N} N - 1}{2(N-1)} \right]\!\right]_{\overline{N}} \qquad (32)$$
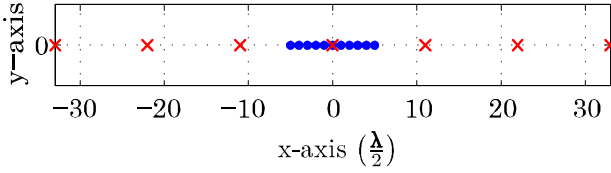
For sufficiently large receive arrays ($N \gg 1$), it is clear that $\overline{N}_{\mathrm{sub}}^{\mathrm{opt}}$ is given by the nearest valid integer to $\frac{\overline{N}}{2}$. In fact, if $\overline{N}$ is even-valued and $N \geq 3$, a useful rule of thumb is that using two subarrays is always optimal:

$$\left.\begin{array}{r} \overline{N}_{\mathrm{sub}}^{\mathrm{opt}} = \frac{\overline{N}}{2} \\ \overline{B}_{\mathrm{sub}}^{\mathrm{opt}} = 2 \end{array}\right\} \quad \begin{array}{l} \text{if } N \geq 3 \\ \text{and } \overline{N} \text{ is even} \end{array} \qquad (33)$$
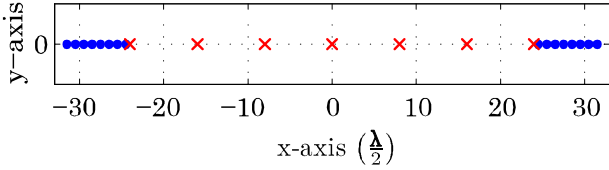
An illustrative example is given in Figure 4. In general, as array sizes become large, it can be shown that the proposed method allows radar platform size to be reduced by up to a half.

If $\overline{N}$ is odd (or, in particular, if it is prime) then spatial efficiency may be especially poor. For example, it is shown

in Figure 5 that a MIMO radar with $(\overline{N} \times N) = (7 \times 11)$ requires a (marginally) *larger* radar platform than is required for $(\overline{N} \times N) = (7 \times 16)$, despite providing a significantly *smaller* virtual aperture ($\overline{N}N = 77$, compared to 112).

(a) Optimal configuration for $(\overline{N} \times N) = (11 \times 7)$. A physical MIMO aperture of 66 half-wavelengths provides a 77-element virtual array.

(b) Optimal configuration for $(\overline{N} \times N) = (16 \times 7)$. A physical MIMO aperture of 63 half-wavelengths provides a 112-element virtual array.

Fig. 5: Linear arrays comprising prime numbers of antennas are particularly spatially inefficient. Blue '·' denotes transmit antenna and red 'x' denotes receive antenna.

V. CONCLUSION

In this paper, an equivalent 'virtual' SIMO (Single Input Multiple Output) radar representation of the MIMO radar system was established. Contrary to the existing literature, this representation allowed the properties of the virtual SIMO system to be identified and analysed without making any specific assumptions about how the structure might be exploited in practice. The fundamental performance capabilities of the MIMO radar configuration were investigated using differential geometry.

A new family of subarrayed linear MIMO array structures was presented. It was shown that, given a limited amount of available space on the radar platform, this approach allowed significantly larger virtual arrays to be realised, compared to traditional methods.

APPENDIX A
PROOF OF EQUATION 7

In this appendix, the following relationships will be used:

$$\underline{a}^H \underline{b} = \left(\underline{a}^* \odot \underline{b}\right)^T \underline{1} \tag{34}$$

$$\mathrm{vec}\left(\mathbb{A}\mathbb{B}\mathbb{C}\right) = \left(\mathbb{C}^T \otimes \mathbb{A}\right)\mathrm{vec}\left(\mathbb{B}\right) \tag{35}$$

$$(\underline{a} \odot \underline{b}) \otimes (\underline{c} \odot \underline{d}) = (\underline{a} \otimes \underline{c}) \odot (\underline{b} \otimes \underline{d}) \tag{36}$$

Thus, we proceed by rearranging Equation 5 as follows (where a number above an equals sign denotes the relevant relationship):

$$\underline{x}(t) = \sum_{k=1}^{K} \beta_k \exp(j2\pi\mathcal{F}_k t)\underline{S}_k \overline{\underline{S}}_k^H \underline{m}(t)c(t-\tau_k) + \underline{n}(t)$$

$$\stackrel{(34)}{=} \sum_{k=1}^{K} \beta_k \exp(j2\pi\mathcal{F}_k t)\underline{S}_k \left(\overline{\underline{S}}_k^* \odot \underline{m}(t)\right)^T \underline{1}_{\overline{N}}c(t-\tau_k) + \underline{n}(t)$$

$$\stackrel{(35)}{=} \sum_{k=1}^{K} \beta_k \exp(j2\pi\mathcal{F}_k t)\left(\underline{1}_{\overline{N}}^T \otimes \mathbb{I}_N\right)\cdot$$
$$\mathrm{vec}\left(\underline{S}_k 1\left(\overline{\underline{S}}_k^* \odot \underline{m}(t)\right)^T\right)c(t-\tau_k) + \underline{n}(t)$$

$$\stackrel{(35)}{=} \sum_{k=1}^{K} \beta_k \exp(j2\pi\mathcal{F}_k t)\left(\underline{1}_{\overline{N}}^T \otimes \mathbb{I}_N\right)\cdot$$
$$\left(\left(\overline{\underline{S}}_k^* \odot \underline{m}(t)\right) \otimes (\underline{S}_k \odot \underline{1}_N)\right)c(t-\tau_k) + \underline{n}(t)$$

$$\stackrel{(36)}{=} \sum_{k=1}^{K} \beta_k \exp(j2\pi\mathcal{F}_k t)\left(\underline{1}_{\overline{N}}^T \otimes \mathbb{I}_N\right)\cdot$$
$$\left(\left(\overline{\underline{S}}_k^* \otimes \underline{S}_k\right) \odot (\underline{m}(t) \otimes \underline{1}_N)\right)c(t-\tau_k) + \underline{n}(t)$$

which leads directly to Equation 7.

REFERENCES

[1] J. Li and P. Stoica, "MIMO radar with colocated antennas: Review of some recent work," *IEEE Signal Process. Mag.*, vol. 24, pp. 106–114, 2007.

[2] A. Haimovich, R. Blum, and L. Cimini, "MIMO radar with widely separated antennas," *IEEE Signal Process. Mag.*, vol. 25, pp. 116–129, 2008.

[3] A. Manikas, *Differential Geometry in Array Processing.* Imperial College Press, 2004.

[4] I. Bekkerman and J. Tabrikian, "Target Detection and Localization Using MIMO Radars and Sonars," *IEEE Transactions on Signal Processing*, vol. 54, no. 10, pp. 3873 –3883, oct. 2006.

[5] B. Friedlander, "Adaptive Signal Design for MIMO Radar," in *MIMO Radar Signal Processing*, J. Li and P. Stoica, Eds. Wiley, 2009, pp. 193 – 234.

[6] C.-Y. Chen and P. Vaidyanathan, "MIMO Radar Spacetime Adaptive Processing and Signal Design," in *MIMO Radar Signal Processing*, J. Li and P. Stoica, Eds. Wiley, 2009, pp. 235 – 281.

[7] J. Zhang and A. Papandreou-Suppappola, "MIMO Radar with Frequency Diversity," in *Waveform Diversity and Design Conference, 2009 International*, feb. 2009, pp. 208 –212.

[8] B. Friedlander, "On the Relationship Between MIMO and SIMO Radars," *IEEE Transactions on Signal Processing*, vol. 57, no. 1, pp. 394 –398, jan. 2009.

[9] H. L. V. Trees, *Optimum Array Processing: Detection, Estimation and Modulation Theory, Part IV.* Wiley, 2002.

[10] G. Efstathopoulos and A. Manikas, "Extended Array Manifolds: Functions of Array Manifolds," *IEEE Transactions on Signal Processing*, vol. 59, no. 7, pp. 3272 –3287, july 2011.

[11] H. Commin and A. Manikas, "Spatiotemporal Arrayed MIMO Radar: Joint Doppler, Delay and DoA Estimation," *IEEE Transactions on Signal Processing*, 2012 [Submitted].

[12] J. Li, P. Stoica, and X. Zheng, "Signal Synthesis and Receiver Design for MIMO Radar Imaging," *IEEE Transactions on Signal Processing*, vol. 56, no. 8, pp. 3959 –3968, aug. 2008.

[13] H. Commin and A. Manikas, "The Figure of Merit "C" for Comparing Superresolution Direction-Finding Algorithms," in *Sensor Signal Processing for Defence (SSPD)*, 2010.